Supplement of

Molecular compositions and optical properties of dissolved brown carbon in smoke particles illuminated by excitation-emission matrix spectroscopy and Fourier-transform ion cyclotron resonance mass spectrometry (FT-ICR MS) analysis

Jiao Tang et al.

Correspondence to: Gan Zhang (Zhanggan@gig.ac.cn) and Jun Li (junli@gig.ac.cn)

Contents:

S1. Data analysis.

Emission factors

Fuel-based emission factors were obtained by the carbon mass balance formula:(Cui et al., 2018;Cui et al., 2017)

$$\mathrm{EF}_i = \frac{\Delta X_i}{\Delta CO_2} \cdot \frac{M_i}{M_{CO_2}} \cdot EF_{CO_2} \quad (1)$$

Here, EF_i and EF_{CO_2}(g kg^{-1} fuel) are the emission factor for species *i* and CO_2, respectively. ΔX_i and ΔCO_2 (mol m^{-3}), as well as M_i and M_{CO_2}(g mol^{-1}) are the background-corrected concentrations and molecular weights of species *i* and CO_2, respectively.

Among the above formula, the CO_2 emission factor (EF_{CO_2}) were calculated as:

$$EF_{CO_2} = \frac{C_F}{c(C_{CO}) + c(C_{CO_2}) + c(C_{PM})} \cdot c(CO_2) \cdot M_{CO_2} \quad (2)$$

Here, C_F (g C kg^{-1} fuel) are the mass of carbon in 1kg diesel fuel; $c(C_{CO})$, $c(C_{CO2})$ and $c(C_{PM})$ (g C m^{-3}) are the corresponding flue gas mass concentrations of carbon, respectively; $c(CO_2)$ (mol m^{-3}) is the molar concentration of CO_2.

ESI FT-ICR MS data processing

Custom software was applied to calculate all mathematically possible formulas for all ions with a signal-to-noise ratio > 10 using a mass tolerance of ± 1.5 ppm as described elsewhere (Mo et al., 2018;Lin et al., 2015). Formula calculator was performed using the following constraints: C ≤ 45, H ≤ 60, O ≤ 20, N ≤ 3, and S ≤ 2. Identified formulas with isotopomers (i.e., ^{13}C, ^{18}O, or ^{34}S) were not discussed in this paper. These identified molecular formulas were classified into four main compound groups based on their composition: CHO, CHON, CHOS, and CHONS compounds. For the chemical formula $C_cH_hO_oN_nS_s$, the double bonds equivalent (DBE) used as measure of unsaturated level in a molecule was calculated using the following equation: DBE = (2c + 2 – h + n)/2, and an aromaticity index (AI) used to estimate the

fraction of aromatic and condensed aromatic structures was calculated to estimate the fraction of aromatic and condensed aromatic structures from the formulas: AI_{mod} = (1 + c – 0.5o – s – 0.5h)/(c – 0.5o – s – n) (Song et al., 2018). Commonly, formulae are as follows: no aromatic (AI_{mod} < 0.5), aromatic (AI_{mod} >0.5) and condensed aromatic (AI_{mod} ≥ 0.67). The van Krevelen (VK) diagram was a useful tool which could provide a visual graphic display of compound distribution (Lv et al., 2016).

From the molecular formula assignments, the intensity-averaged calculations for each sample can be determined by the following equations:(Mo et al., 2018;Song et al., 2018;Lv et al., 2016)

$$O/Cw= \Sigma(w_i*o_i)/ \Sigma(w_i*c_i) \quad (3)$$

$$H/Cw= \Sigma(w_i*hi)/ \Sigma(w_i*c_i) \quad (4)$$

$$DBEw= \Sigma(w_i*DBE_i)/ \Sigma w_i \quad (5)$$

$$AI_{mod,w}=\Sigma(w_i*AI_{mod,i})/ \Sigma w_i \quad (6)$$

Where, w_i is the relative abundance for each individual molecular formula, *i*.

S2. Quality control

In this study, the field blank values of TC (TC=OC+EC), WSOC, and MSOC for ambient blank sample were 0.75 ± 0.02 μg C cm^{-2}, 1.2 ± 0.21 μg C cm^{-2}, 0.48 μg C cm^{-2}, respectively. The standard deviation of parallel experiments based on smoke particle samples were 0.01 μg C cm^{-2}, 0.14 μg C mL^{-1}, 0.16 μg C mL^{-1} for TC, WSOC, and MSOC, respectively. We also corrected the procedural blank concentrations of WSOC and MSOC in each sample. The total recoveries of WSOC and MSOC to OC were 112 % ± 14 % for biomass burning, 101 % ± 20 % for coal combustion, and 100 % ± 26 % for vehicle emission.

The value of absorbance for field blank samples at 365 nm was 0.0009 ± 0.00008, much less than that of smoke samples. The standard deviation of parallel experiments of absorbance at 365 nm for instrument and method were 0.00006 and 0.0008, respectively. Further, no obvious peak was found in the fluorescence spectrum of field blank samples. The fluorescence spectrum of samples were measured with their absorbance lower than 1.

Reference:

Chen, Q., Ikemori, F., Nakamura, Y., Vodicka, P., Kawamura, K., and Mochida, M.: Structural and Light-Absorption Characteristics of Complex Water-Insoluble Organic Mixtures in Urban Submicrometer Aerosols, Environ. Sci. Technol., 51, 8293-8303, https://doi.org/10.1021/acs.est.7b01630., 2017.

Chen, Y., Ge, X., Chen, H., Xie, X., Chen, Y., Wang, J., Ye, Z., Bao, M., Zhang, Y., and Chen, M.: Seasonal light absorption properties of water-soluble brown carbon in atmospheric fine particles in Nanjing, China, Atmos. Environ., 230-240, https://doi.org/10.1016/j.atmosenv.2018.06.002, 2018.

Cui, M., Chen, Y., Feng, Y., Li, C., Zheng, J., Tian, C., Yan, C., and Zheng, M.: Measurement of PM and its chemical composition in real-world emissions from non-road and on-road diesel vehicles, Atmos. Chem. Phys., 17, 6779-6795, https://doi.org/10.5194/acp-17-6779-2017, 2017.

Cui, M., Chen, Y., Zheng, M., Li, J., Tang, J., Han, Y., Song, D., Yan, C., Zhang, F., Tian, C., and Zhang, G.: Emissions and characteristics of particulate matter from rainforest burning in the Southeast Asia, Atmos. Environ., 191, 194-204, https://doi.org/10.1016/j.atmosenv.2018.07.062, 2018.

Li, M., Fan, X., Zhu, M., Zou, C., Song, J., Wei, S., Jia, W., and Peng, P.: Abundances and light absorption properties of brown carbon emitted from residential coal combustion in China, Environ. Sci. Technol., 53, 595-603, https://doi.org/10.1021/acs.est.8b05630, 2018.

Lin, P., Laskin, J., Nizkorodov, S. A., and Laskin, A.: Revealing Brown Carbon Chromophores Produced in Reactions of Methylglyoxal with Ammonium Sulfate, Environ. Sci. Technol., 49, 14257-14266, https://doi.org/10.1021/acs.est.5b03608, 2015.

Liu, J., Mo, Y., Ding, P., Li, J., Shen, C., and Zhang, G.: Dual carbon isotopes ((14)C and (13)C) and optical properties of WSOC and HULIS-C during winter in Guangzhou, China, Sci. Total Environ., 633, 1571-1578, https://doi.org/10.1016/j.scitotenv.2018.03.293, 2018.

Lv, J., Zhang, S., Wang, S., Luo, L., Cao, D., and Christie, P.: Molecular-Scale Investigation with ESI-FT-ICR-MS on Fractionation of Dissolved Organic Matter Induced by Adsorption on Iron Oxyhydroxides, Environ. Sci. Technol., 50, 2328-2336, https://doi.org/10.1021/acs.est.5b04996, 2016.

Mo, Y., Li, J., Jiang, B., Su, T., Geng, X., Liu, J., Jiang, H., Shen, C., Ding, P., Zhong, G., Cheng, Z., Liao, Y., Tian, C., Chen, Y., and Zhang, G.: Sources, compositions, and optical properties of humic-like substances in Beijing during the 2014 APEC summit: Results from dual carbon isotope and Fourier-transform ion cyclotron resonance mass spectrometry analyses, Environ. Pollut., 239, 322-331, https://doi.org/10.1016/j.envpol.2018.04.041, 2018.

Park, S. S., and Yu, J.: Chemical and light absorption properties of humic-like substances from biomass burning emissions under controlled combustion experiments, Atmos. Environ., 136, 114-122, https://doi.org/10.1016/j.atmosenv.2016.04.022, 2016.

Patriarca, C., Bergquist, J., Sjoberg, P. J. R., Tranvik, L., and Hawkes, J. A.: Online HPLC-ESI-HRMS Method for the Analysis and Comparison of Different Dissolved Organic Matter Samples, Environ. Sci. Technol., 52, 2091-2099, https://doi.org/10.1021/acs.est.7b04508, 2018.

Song, J., Li, M., Jiang, B., Wei, S., Fan, X., and Peng, P.: Molecular Characterization of Water-Soluble Humic like Substances in Smoke Particles Emitted from Combustion of Biomass Materials and Coal Using Ultrahigh-Resolution Electrospray Ionization Fourier Transform Ion Cyclotron Resonance Mass Spectrometry, Environ. Sci. Technol., 52, 2575-2585, https://doi.org/10.1021/acs.est.7b06126, 2018.

Yan, C., Zheng, M., Sullivan, A. P., Bosch, C., Desyaterik, Y., Andersson, A., Li, X., Guo, X., Zhou, T., Gustafsson, Ö., and Collett, J. L.: Chemical characteristics and light-absorbing property of water-soluble organic carbon in Beijing: Biomass burning contributions, Atmos. Environ., 121, 4-12, https://doi.org/10.1016/j.atmosenv.2015.05.005, 2015.

Zhu, C. S., Cao, J. J., Huang, R. J., Shen, Z. X., Wang, Q. Y., and Zhang, N. N.: Light absorption properties of brown carbon over the southeastern Tibetan Plateau, Sci. Total Environ., 625, 246-251, https://doi.org/10.1016/j.scitotenv.2017.12.183, 2018.

Table S1. Elemental analysis of 27 main biomass types.

IDs	Latin name	Biomass types			
		N%	C%	H%	O%
1	Eupatorium odoratum L.	0.97	42	6.0	39
2	Chaetocarpus castanocarpus	1.9	46	5.7	41
3	Cassia siamea Lam.	2.3	38	5.5	33
4	Baccaurea ramiflora Lour.	1.5	48	6.3	46
5	Rauvolfieae verticillata*	0.32	49	6.0	46
6	Macaranga denticulata	0.91	49	6.4	46
7	Toona ciliata M. Roem.	0.51	43	7.1	44
8	Duabanga grandiflora	0.46	44	5.8	45
9	Paramichelia baillonii	0.00	48	6.1	49
10	Bischofia polycarpa	0.38	48	6.7	45
11	Rauvolfieae verticillata	0.78	48	6.2	47
12	Pseudostachyum polymorphum	0.71	44	6.6	47
13	Broussonetia papyrifera	0.65	49	7.3	48
14	Citrus maxima	0.66	51	5.7	45
15	Litchi chinensis Sonn.	0.62	46	6.3	44
16	Anthocephalus chinensis	1.6	45	5.7	44
17	Antiaris toxicaria Lesch.	1.0	46	5.9	47
18	Musa nana Lour.	0.86	50	6.8	46
19	Melia azedarach	0.69	47	5.8	48
20	Pterospermum menglunense Hsue	0.72	46	5.3	56
21	Castanopsis Spach	0.73	50	5.7	24
22	Rhynchelytrum repens	0.33	49	5.9	73
23	Hevea brasiliensis	0.41	49	5.9	49
24	Trema tomentosa (Roxb.) H. Hara	0.49	47	5.5	50
25	Pinus kesiya var. langbianensis	0.42	39	5.5	49
26	Lasiococca comberi Haines H. S. Kiu	0.95	46	5.4	51

27	Broussonetia papyrifera*	1.4	37	5.1	48

Note that the “*” is representative of twig of this tree.

Table S2. Elemental analysis of 17 main coal types.

Types	IDs	Location	N%	C%	H%	O%	S%
Anthracite	34	Jining	0.51	75	3.4	6.2	0.29
	35	Yangcheng	0.39	75	3.5	5.1	0.00
	36	Liupanshui	0.73	80	3.5	4.5	0.20
	37	Menkou	0.57	85	3.1	5.5	0.00
	38	Xinxiang	0.61	86	3.3	5.2	0.00
	39	Chengzhou	0.65	77	3.3	5.0	0.09
	40	Yinchuan	0.18	91	4.3	3.8	0.00
Bituminous coal	41	Huainan	0.47	75	4.1	20	0.00
	42	Baitashan	0.30	68	3.9	29	0.00
	43	Longkou	1.0	65	4.8	27	0.19
	44	Baoji	0.25	68	4.0	21	0.00
	45	Lingshi	0.78	81	4.4	6.0	0.77
	46	Dazhou	0.44	76	3.3	6.9	0.30
	47	Shenmu	0.59	77	4.4	14	0.00
	48	Daqing	0.37	69	5.0	19	0.00
	49	Zibo	0.46	76	3.7	5.4	0.73
	50	Hailaer	0.58	64	4.7	30	0.00

Table S3. The EFs of 27 biomass burning and 17 coal combustion and carbon content of three origins.

	Biomass burning		Anthracite combustion		Bituminous coal combustion		Vehicle emission	
	Avg	SD	Avg	SD	Avg	SD	Avg	SD
PM (g kg^{-1} fuel)	15	11	1.5×10^{-1}	8.9×10^{-2}	9.1×10^{-1}	6.5×10^{-1}	3.7 [a]	7.8 [a]
OC(g kg^{-1} fuel)	8.0	6.4	1.2×10^{-2}	4.5×10^{-3}	4.2×10^{-1}	3.3×10^{-1}	3.7×10^{-1} [a]	8.2×10^{-1} [a]
EC (g kg^{-1} fuel)	7.7×10^{-1}	3.4×10^{-1}	1.6×10^{-4}	1.4×10^{-4}	9.4×10^{-2}	1.9×10^{-1}	1.0×10^{-1} [a]	2.2×10^{-1} [a]
WSOC (μg C mL^{-1})	4.8	2.6	1.1	1.9×10^{-1}	3.2	3.7	2.6	1.8
MSOC (μg C mL^{-1})	8.5	10	1.1	1.0	25	26	2.5	1.1
WSOC/OC	0.50	0.15	0.66	0.18	0.13	0.08	0.45	0.11
MSOC/OC	0.62	0.18	0.47	0.14	0.80	0.20	0.56	0.25
OC/EC	16	32	145	99	21	28	3.0	1.5

Note: a, units (mg C m^{-3}).

Table S4. Mass absorption efficiency at 365 nm in different extracts of three origins.

	MAE_{365} (m^2 g^{-1} C)		Reference
Extracts	WSOC	MSOC	
Biomass burning	1.6 ± 0.55	2.3 ± 1.1	In current study
Anthracite combustion	1.3 ± 0.34	0.88 ± 0.74	
Bituminous coal combustion	2.0 ± 0.75	3.2 ± 1.1	
Vehicle emission	0.71 ± 0.30	0.26 ± 0.09	
Smoke particle from coal combustion	0.3 - 0.7 for bituminous coal, 0.9 - 1.0 for anthracite		(Li et al., 2018)
$PM_{2.5}$ from biomass burning	0.86 - 1.38		(Park and Yu, 2016)
$PM_{2.5}$	1.54 ± 0.16 (Winter) 0.73 ± 0.15 (summer)		(Yan et al., 2015)
Total suspended particulate	0.75 ± 0.13 (winter)		(Zhu et al., 2018)
$PM_{2.5}$	0.51 - 1.04		(Chen et al., 2018)
PM (aerodynamic diameter: <0.95 μm)	< 0.4		(Chen et al., 2017)
Total suspended particulate	0.81 ± 0.16		(Liu et al., 2018)

Table S5. The maximum fluorescence intensities (RU) of P1-P6 of WSOC fraction in three origins.

	P1 (Avg ± SD)	P2 (Avg ± SD)	P3 (Avg ± SD)	P4 (Avg ± SD)	P5 (Avg ± SD)	P6 (Avg ± SD)
Biomass burning	41 ± 42	$92 \pm 1.2\times10^{2}$	30 ± 26	23 ± 47	48 ± 64	4.0 ± 4.5
Coal combustion	57 ± 76	68 ± 90	65 ± 84	$1.1\times10^{2} \pm 1.2\times10^{2}$	72 ± 88	6.5 ± 9.2
vehicle emission	6.0 ± 3.1	0 ± 0	2.6 ± 2.0	5.1 ± 1.7	3.5 ± 1.7	1.9 ± 1.3
Total	39 ± 53	$70 \pm 1.1\times10^{2}$	35 ± 52	44 ± 83	47 ± 69	4.3 ± 6.1

Table S6. The maximum fluorescence intensities (RU) of C1-C6 of MSOC fraction in three origins.

	C1 (Avg ± SD)	C2 (Avg ± SD)	C3 (Avg ± SD)	C4 (Avg ± SD)	C5 (Avg ± SD)	C6 (Avg ± SD)
Biomass burning	1.9×10^{2} ± 4.3×10^{2}	1.2×10^{2} ± 2.9×10^{2}	80 ± 2.3×10^{2}	1.2×10^{2} ± 4.0×10^{2}	95 ± 2.4×10^{2}	37 ± 97
Coal combustion	1.2×10^{3} ± 1.3×10^{3}	1.4×10^{3} ± 1.8×10^{3}	1.5×10^{3} ± 2.1×10^{3}	5.2×10^{3} ± 7.8×10^{3}	1.5×10^{3} ± 2.4×10^{3}	6.3×10^{2} ± 1.1×10^{3}
vehicle emission	6.6 ± 6.3	8.5 ± 8.0	5.7 ± 4.9	15 ± 13	6.9 ± 5.1	11 ± 6.5
Total	4.5×10^{2} ± 9.1×10^{2}	4.7×10^{2} ± 1.1×10^{3}	4.7×10^{2} ± 1.3×10^{3}	1.5×10^{3} ± 4.7×10^{3}	4.9×10^{2} ± 1.4×10^{3}	2.0×10^{2} ± 6.3×10^{2}

Table S7. The number of formulas identified for each compound class and average values of molecular weight, elemental ratios, double-bond equivalent (DBE) and aromaticity index (AI_{mod}) in WSOC fraction from three origins.

Origins	Samples	Elemental compositions	number of formulas	Molecular weight	O/C_W	H/C_W	$AI_{mod,W}$	DBE_W
Biomass burning	B18	CHO	2362	341	0.39	1.3	0.29	7.1
		CHON	2970	387	0.35	1.2	0.39	9.4
		CHOS	430	328	0.40	1.5	0.15	4.6
		CHONS	330	359	0.55	1.5	0.13	5.1
	B23	CHO	1975	357	0.39	1.16	0.39	9.1
		CHON	1536	390	0.41	1.1	0.46	11
		CHOS	171	351	0.30	1.5	0.21	6.1
		CHONS	56	401	0.65	1.4	0.27	5.8
Coal combustion	C38	CHO	1302	281	0.29	0.89	0.60	10.0
		CHON	1984	322	0.36	0.83	0.70	11
		CHOS	552	316	0.34	1.2	0.37	7.2
		CHONS	741	338	0.52	0.96	0.52	9.2
	C46	CHO	600	263	0.22	1.0	0.53	8.5
		CHON	478	267	0.28	0.93	0.65	9.4
		CHOS	396	326	0.27	1.3	0.35	7.4
		CHONS	291	306	0.49	0.98	0.57	8.0
Vehicle emission	SD55	CHO	1107	289	0.50	1.2	0.40	6.7
		CHON	1202	340	0.52	1.2	0.38	7.7
		CHOS	578	313	0.59	1.7	0.04	2.8
		CHONS	403	340	0.91	1.8	0.45	2.8
	SD59	CHO	910	289	0.28	1.4	0.29	5.5
		CHON	803	317	0.40	1.3	0.38	6.9
		CHOS	119	372	0.24	1.5	0.24	7.1

	CHONS	15	384	0.93	1.01	0.76	7.0

149

Table S8. The number of formulas identified for each compound class and average values of molecular weight, elemental ratios, double-bond equivalent (DBE) and aromaticity index (AI_{mod}) in MSOC fraction from three origins.

Origins	Samples	Elemental compositions	number of formulas	Molecular weight	O/C_W	H/C_W	$AI_{mod,W}$	DBE_W
Biomass burning	B18	CHO	1890	365	0.14	1.8	0.11	3.2
		CHON	1255	425	0.17	1.7	0.18	5.2
		CHOS	100	367	0.20	1.7	0.10	3.5
		CHONS	49	460	0.32	1.7	0.09	4.5
	B23	CHO	1401	349	0.19	1.6	0.20	4.9
		CHON	306	322	0.12	1.9	0.10	2.5
		CHOS	59	333	0.22	1.7	0.12	3.5
		CHONS	14	423	0.31	1.9	0.07	2.8
Coal combustion	C38	CHO	600	295	0.17	1.4	0.31	5.8
		CHON	1097	312	0.21	1.2	0.48	8.2
		CHOS	99	334	0.24	1.6	0.15	4.1
		CHONS	54	366	0.66	1.4	0.42	5.0
	C46	CHO	1071	334	0.12	1.0	0.54	12
		CHON	898	341	0.17	1.1	0.56	11
		CHOS	240	346	0.24	1.3	0.37	8.2
		CHONS	19	385	0.69	0.93	0.56	9.4
Vehicle emission	SD55	CHO	480	320	0.16	1.9	0.07	1.8
		CHON	237	377	0.21	2.0	0.04	1.7
		CHOS	170	360	0.30	1.8	0.06	2.6
		CHONS	50	341	0.81	1.8	0.51	3.1
	SD59	CHO	310	314	0.14	2.0	0.04	1.3
		CHON	217	340	0.13	1.9	0.08	2.1
		CHOS	43	362	0.19	1.8	0.09	3.1
		CHONS	13	418	0.44	1.5	0.36	6.1

Table S9. The first method is to follow their O/C and H/C ratios of matter to classify all ions of FT-ICR MS: The Pearson's correlation coefficients (r) and the significance levels (p, two-sided t-test) from the correlation analysis between the relative intensity of the PARAFAC components and the FT-ICR MS ions-groups for WSOC fractions in three origins (n=6).

		Lipids	Proteins	H-Lignin	M-Lignin	L-Lignin	Carbohydrates	Tannins	Unsaturated hydrocarbons
P1	*r*	-0.63	0.42	-0.69	0.43	-0.69	0.79	0.73	-0.78
	p	0.18	0.41	0.13	0.40	0.13	0.06	0.10	0.07
P2	*r*	-0.31	-0.66	0.41	0.32	-0.39	-0.48	-0.34	0.27
	p	0.56	0.15	0.42	0.54	0.45	0.34	0.51	0.61
P3	*r*	-0.60	-0.32	0.18	0.59	-0.73	-0.34	-0.04	-0.37
	p	0.21	0.54	0.73	0.22	0.10	0.52	0.94	0.47
P4	*r*	0.45	-0.17	0.53	**-0.87***	0.70	-0.16	0.02	0.40
	p	0.37	0.74	0.28	0.02	0.12	0.76	0.97	0.44
P5	*r*	0.75	0.32	-0.16	0.07	0.70	-0.34	-0.76	0.55
	p	0.09	0.54	0.76	0.89	0.15	0.51	0.08	0.26
P6	*r*	-0.35	0.48	-0.67	0.24	-0.52	0.79	0.72	**-0.82***
	p	0.50	0.34	0.14	0.64	0.29	0.06	0.11	0.04

**. P<0.01;*.p<0.05

Table S10. The first method is to follow their O/C and H/C ratios of matter to classify all ions of FT-ICR MS: The Pearson's correlation coefficients (r) and the significance levels (p, two-sided t-test) from the correlation analysis between the relative intensity of the PARAFAC components and the FT-ICR MS ions-groups for MSOC fractions in three origins (n=6).

		Lipids	Proteins	H-Lignin	M-Lignin	L-Lignin	Carbohydrates	Tannins	Unsaturated hydrocarbons
C1	*r*	-0.11	-0.66	0.20	0.80	0.02	-0.37	-0.24	-0.21
	p	0.84	0.15	0.71	0.05	0.97	0.47	0.65	0.70
C2	*r*	-0.34	-0.31	0.34	0.64	0.06	0.12	0.02	0.11
	p	0.51	0.55	0.51	0.18	0.91	0.82	0.97	0.84
C3	*r*	0.05	-0.13	-0.03	0.55	0.06	0.30	0.04	-0.25
	p	0.93	0.80	0.96	0.26	0.91	0.57	0.95	0.64
C4	*r*	-0.53	0.27	0.59	-0.05	0.64	0.04	0.70	0.36
	p	0.28	0.60	0.22	0.92	0.17	0.94	0.12	0.48
C5	*r*	0.38	0.36	-0.46	-0.61	-0.20	0.01	-0.10	-0.09
	p	0.45	0.49	0.36	0.20	0.70	0.99	0.85	0.87
C6	*r*	0.37	0.37	-0.46	-0.81	-0.37	0.09	-0.23	0.02
	p	0.47	0.47	0.36	0.05	0.47	0.86	0.67	0.98

**. P<0.01;*.p<0.05

Table S11. The second method is to follow their O/C and H/C ratios of matter to classify potential BrC ions: The Pearson's correlation coefficients (r) and the significance levels (p, two-sided t-test) from the correlation analysis between the relative intensity of the PARAFAC components and the FT-ICR MS ions-groups for WSOC fractions in three origins (n=6).

		Lipids	Proteins	H-Lignin	M-Lignin	L-Lignin	Carbohydrates	Tannins	Unsaturated hydrocarbons
P1	*r*		0.35	**-0.89***	0.59		0.31	0.67	-0.75
	p		0.50	0.02	0.22		0.55	0.15	0.09
P2	*r*		0.49	0.24	0.19		-0.34	-0.58	0.15
	p		0.32	0.65	0.71		0.51	0.22	0.78
P3	*r*		0.79	0.06	0.31		-0.59	-0.35	-0.50
	p		0.06	0.91	0.55		0.22	0.49	0.31
P4	*r*		-0.84*	0.61	-0.91*		0.15	0.15	0.43
	p		0.04	0.20	0.01		0.78	0.78	0.40
P5	*r*		-0.06	0.18	0.12		-0.06	-0.51	0.62
	p		0.92	0.73	0.82		0.91	0.31	0.19
P6	*r*		0.03	-0.80	0.44		0.31	0.72	-0.76
	p		0.96	0.06	0.38		0.55	0.11	0.08

**. P<0.01;*.p<0.05

Table S12. The second method is to follow their O/C and H/C ratios of matter to classify potential BrC ions: The Pearson's correlation coefficients (r) and the significance levels (p, two-sided t-test) from the correlation analysis between the relative intensity of the PARAFAC components and the FT-ICR MS ions-groups for MSOC fractions in three origins (n=6).

		Lipids	Proteins	H-Lignin	M-Lignin	L-Lignin	Carbohydrates	Tannins	Unsaturated hydrocarbons
C1	*r*			0.60	0.50			-0.73	-0.21
	p			0.21	0.32			0.10	0.69
C2	*r*			0.28	0.31			-0.69	0.08
	p			0.59	0.55			0.13	0.88
C3	*r*			0.31	0.63			-0.45	-0.28
	p			0.54	0.18			0.37	0.60
C4	*r*			0.19	-0.73			-0.17	0.37
	p			0.71	0.10			0.75	0.47
C5	*r*			-0.42	-0.21			0.74	-0.07
	p			0.41	0.69			0.10	0.90
C6	*r*			-0.64	-0.214			**0.82***	0.02
	p			0.17	0.69			0.05	0.96

**. P<0.01;*.p<0.05

Table S13. The third method is to follow their functional groups to classify all ions: The Pearson's correlation coefficients (r) and the significance levels (p, two-sided t-test) from the correlation analysis between the relative intensity of the PARAFAC components and the FT-ICR MS ions-groups for WSOC fractions in three origins (n=6).

		CHO_1	$CHO_{>1}$	L-CHON	H-CHON	L-CHOS	H-CHOS	L-CHONS	H-CHONS
P1	*r*	-0.78	0.22	-0.33	0.29	**-0.90***	0.15	-0.76	0.60
	p	0.07	0.68	0.52	0.58	0.02	0.77	0.08	0.21
P2	*r*	0.28	0.29	0.51	-0.04	0.05	-0.42	0.26	-0.61
	p	0.59	0.58	0.30	0.94	0.93	0.41	0.62	0.20
P3	*r*	-0.44	0.17	0.51	0.77	-0.52	-0.59	-0.18	-0.32
	p	0.38	0.75	0.30	0.08	0.29	0.22	0.73	0.53
P4	*r*	0.36	-0.59	-0.20	-0.19	0.48	0.39	0.57	0.26
	p	0.48	0.22	0.71	0.72	0.34	0.45	0.24	0.62
P5	*r*	0.61	0.14	0.17	-0.47	**0.82***	-0.11	0.21	-0.54
	p	0.20	0.80	0.75	0.35	0.05	0.84	0.69	0.27
P6	*r*	-0.80	0.28	-0.65	0.19	-0.80	0.17	-0.80	0.64
	p	0.06	0.59	0.16	0.72	0.06	0.74	0.06	0.17

**. P<0.01;*.p<0.05

Table S14. The third method is to follow their functional groups to classify all ions: The Pearson's correlation coefficients (r) and the significance levels (p, two-sided t-test) from the correlation analysis between the relative intensity of the PARAFAC components and the FT-ICR MS ions-groups for MSOC fractions in three origins (n=6).

		CHO_1	$CHO_{>1}$	L-CHON	H-CHON	L-CHOS	H-CHOS	L-CHONS	H-CHONS
C1	r	-0.20	0.54	-0.36	-0.39	-0.18	-0.50	-0.37	-0.50
	p	0.70	0.27	0.49	0.44	0.73	0.31	0.48	0.31
C2	r	0.11	0.18	-0.36	-0.06	-0.39	0.11	-0.61	-0.05
	p	0.83	0.73	0.49	0.92	0.44	0.83	0.20	0.92
C3	r	-0.24	0.31	-0.21	-0.17	-0.34	-0.11	-0.36	0.09
	p	0.65	0.55	0.69	0.74	0.51	0.83	0.49	0.87
C4	r	0.38	-0.81	-0.05	**0.94****	0.27	0.56	0.12	0.41
	p	0.45	0.05	0.92	0.01	0.60	0.25	0.81	0.42
C5	r	-0.10	-0.08	0.22	0.00	0.17	-0.06	0.53	0.13
	p	0.84	0.88	0.68	1.00	0.75	0.92	0.28	0.81
C6	r	0.00	-0.08	0.45	-0.20	0.20	0.06	0.38	0.07
	p	0.99	0.89	0.38	0.71	0.71	0.92	0.46	0.90

**. *P<0.01;*.p<0.05*

Table S15. The last method is to follow their functional groups to classify potential BrC ions: The Pearson's correlation coefficients (r) and the significance levels (p, two-sided t-test) from the correlation analysis between the relative intensity of the PARAFAC components and the FT-ICR MS ions-groups for WSOC fractions in three origins (n=6).

		CHO_1	$CHO_{>1}$	L-CHON	H-CHON	L-CHOS	H-CHOS	L-CHONS	H-CHONS
P1	*r*	-0.72	0.65	-0.12	0.48	-0.57	**-0.82***	-0.76	-0.42
	p	0.11	0.16	0.83	0.34	0.24	0.05	0.08	0.41
P2	*r*	0.21	-0.03	0.42	-0.16	-0.34	0.11	0.27	-0.44
	p	0.70	0.96	0.41	0.76	0.51	0.84	0.60	0.39
P3	*r*	-0.52	-0.15	0.50	0.68	-0.68	-0.34	-0.20	-0.05
	p	0.29	0.77	0.31	0.14	0.14	0.51	0.71	0.93
P4	*r*	0.34	-0.47	-0.36	-0.31	0.37	0.61	0.54	**0.85***
	p	0.51	0.35	0.48	0.55	0.47	0.20	0.27	0.03
P5	*r*	0.66	-0.22	0.17	-0.44	**0.84***	0.42	0.24	-0.23
	p	0.16	0.67	0.74	0.38	0.04	0.40	0.64	0.67
P6	*r*	-0.74	0.73	-0.47	0.40	-0.32	**-0.82***	-0.81	-0.25
	p	0.10	0.10	0.35	0.44	0.53	0.05	0.05	0.63

**. $p<0.01$;*.$p<0.05$

Table S16. The last method is to follow their functional groups to classify potential BrC ions: The Pearson's correlation coefficients (r) and the significance levels (p, two-sided t-test) from the correlation analysis between the relative intensity of the PARAFAC components and the FT-ICR MS ions-groups for MSOC fractions in three origins (n=6).

		CHO_1	$CHO_{>1}$	L-CHON	H-CHON	L-CHOS	H-CHOS	L-CHONS	H-CHONS
C1	*r*	-0.20	0.72	-0.01	-0.40	-0.67	**-0.87***	-0.68	-0.73
	p	0.70	0.11	0.99	0.43	0.15	0.02	0.14	0.10
C2	*r*	0.12	**0.87***	-0.01	-0.67	**-0.85***	-0.76	**-0.93****	-0.72
	p	0.83	0.02	0.99	0.15	0.03	0.08	0.01	0.11
C3	*r*	-0.23	**0.94****	-0.24	-0.71	-0.67	-0.80	-0.77	-0.48
	p	0.66	0.01	0.65	0.11	0.15	0.06	0.08	0.34
C4	*r*	0.36	-0.53	0.18	0.59	-0.31	0.09	-0.22	-0.20
	p	0.49	0.28	0.74	0.22	0.56	0.87	0.68	0.71
C5	*r*	-0.11	-0.80	0.11	0.56	**0.84***	0.77	**0.91***	0.77
	p	0.83	0.06	0.83	0.25	0.04	0.08	0.01	0.08
C6	*r*	0.02	-0.61	-0.06	0.26	**0.96****	**0.91***	**0.96****	**0.85***
	p	0.97	0.20	0.91	0.62	0.00	0.01	0.00	0.03

**. P<0.01;*.p<0.05

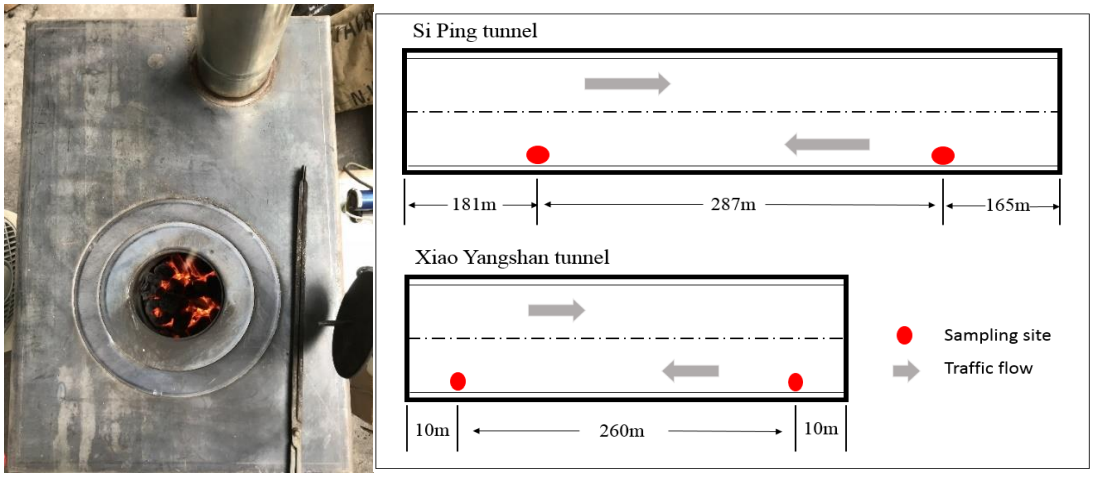

Figure S1. Experiments running in this work (biomass burning, coal combustion, and sampling schematic diagram of tunnel)

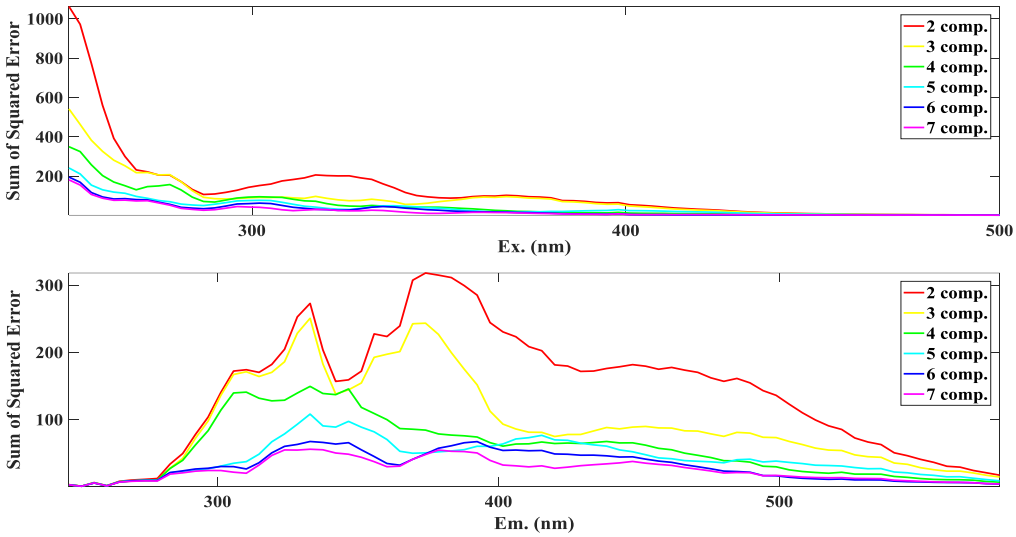

Figure S2. The resident analysis of excitation and emission wavelength of 2- to 7-components PARAFAC model for WSOC fraction

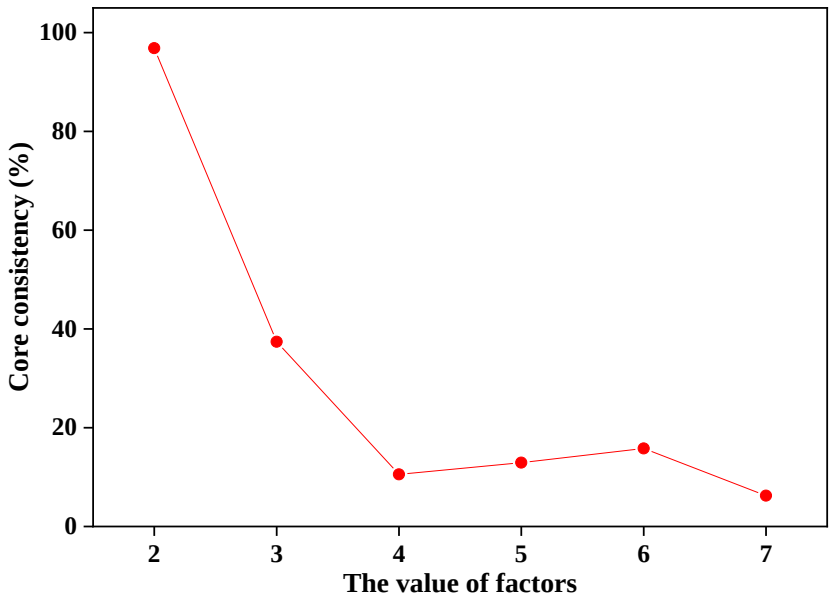

Figure S3. The core consistency of 2- to 7-component model for all EEM of WSOC fraction

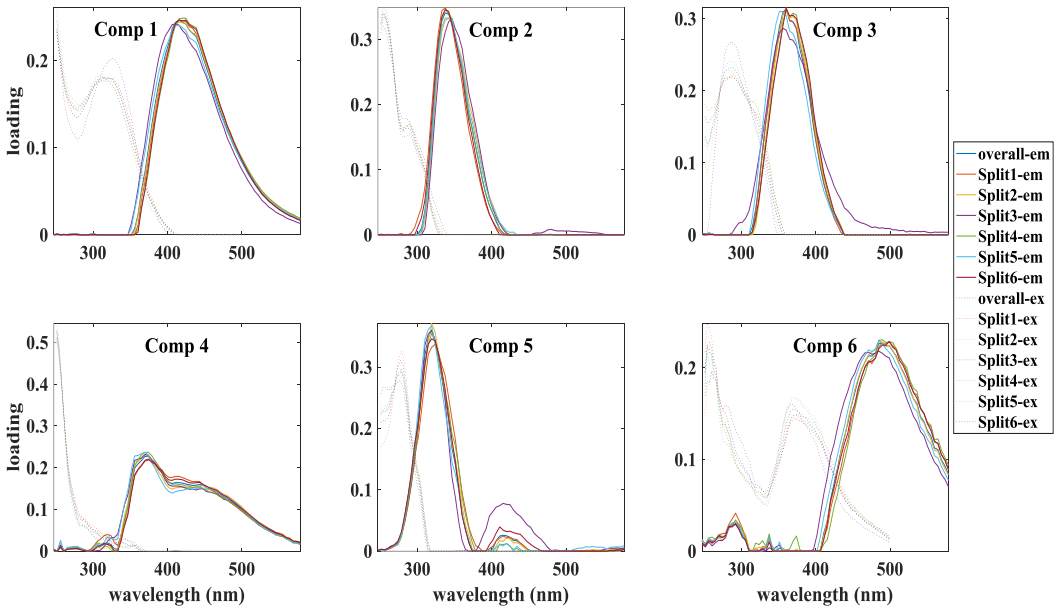

Figure S4. Split analysis of 6-component PARAFAC model with the split style '$S_4C_6T_3$' for all EEM of WSOC fraction

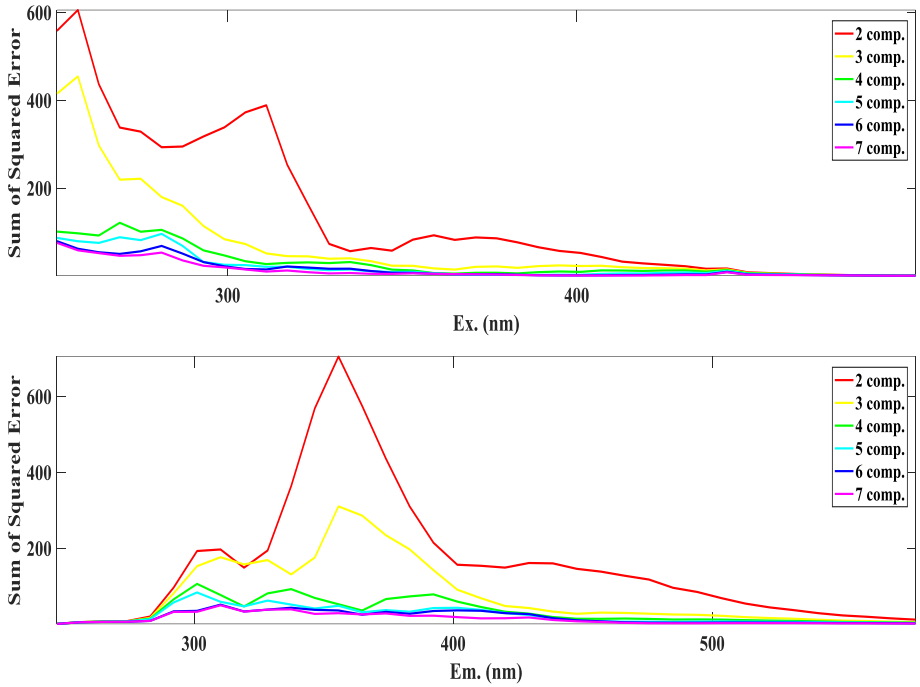

Figure S5. The resident analysis of excitation and emission wavelength of 2- to 7-components PARAFAC model for MSOC fraction

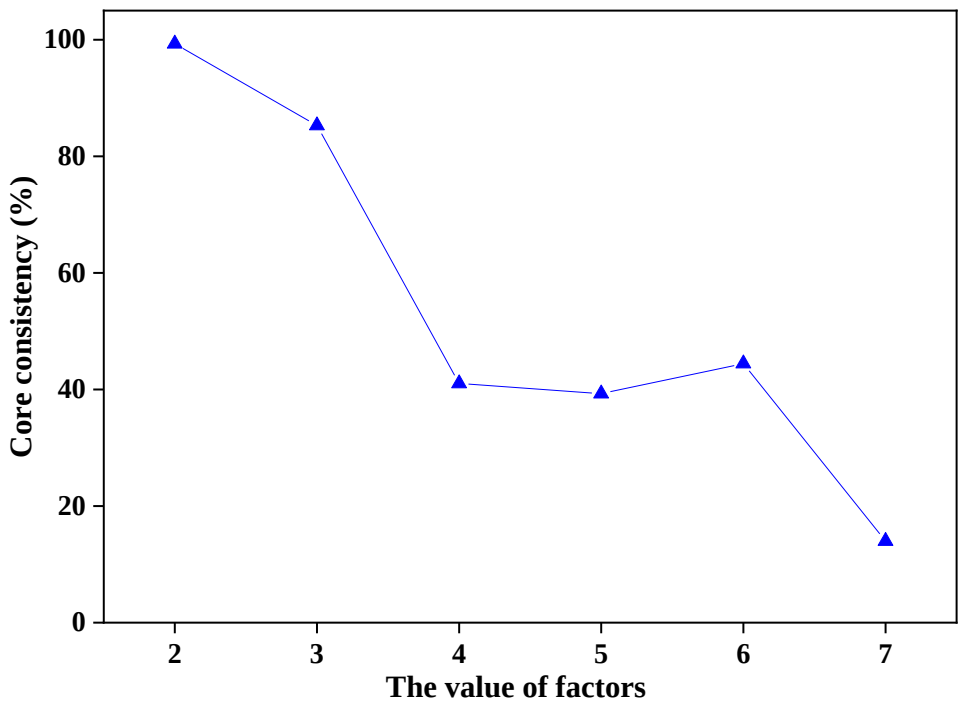

Figure S6. The core consistency of 2- to 7-component model for all EEM of MSOC fraction

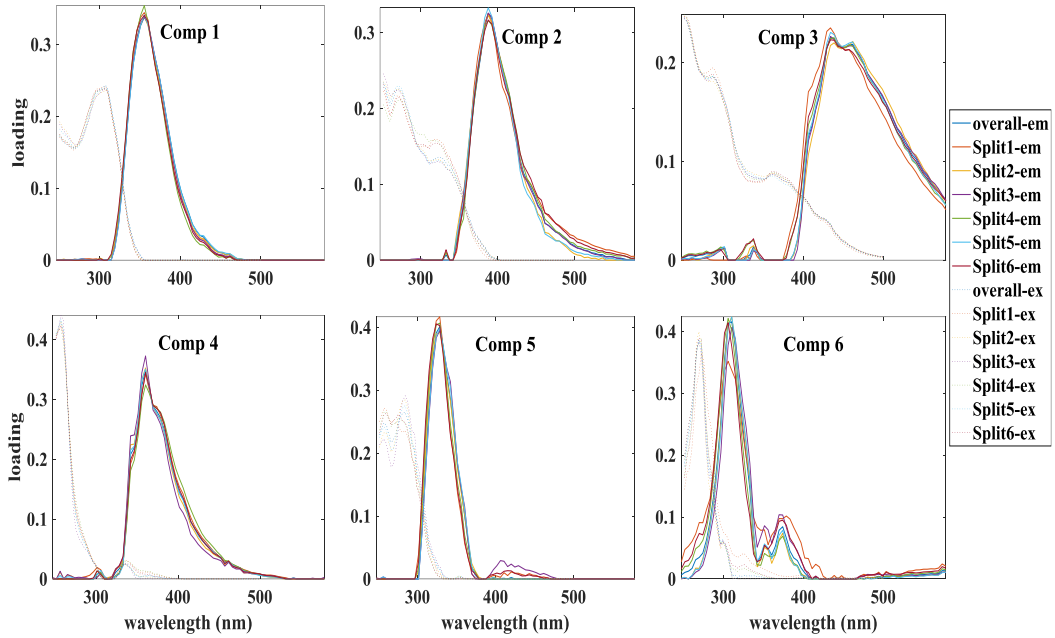

Figure S7. Split analysis of 6-component PARAFAC model with the split style '$S_4C_6T_3$' for all EEM of MSOC fraction

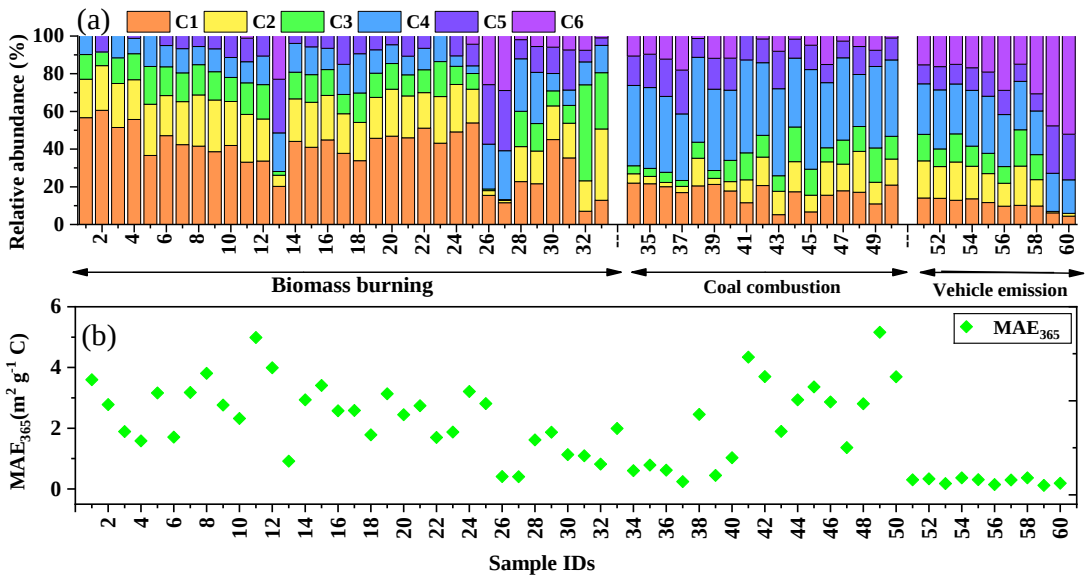

Figure S8. (a) Relative abundance of each PARAFAC component, (b) MAE_{365} values of MSOC fraction of three origins

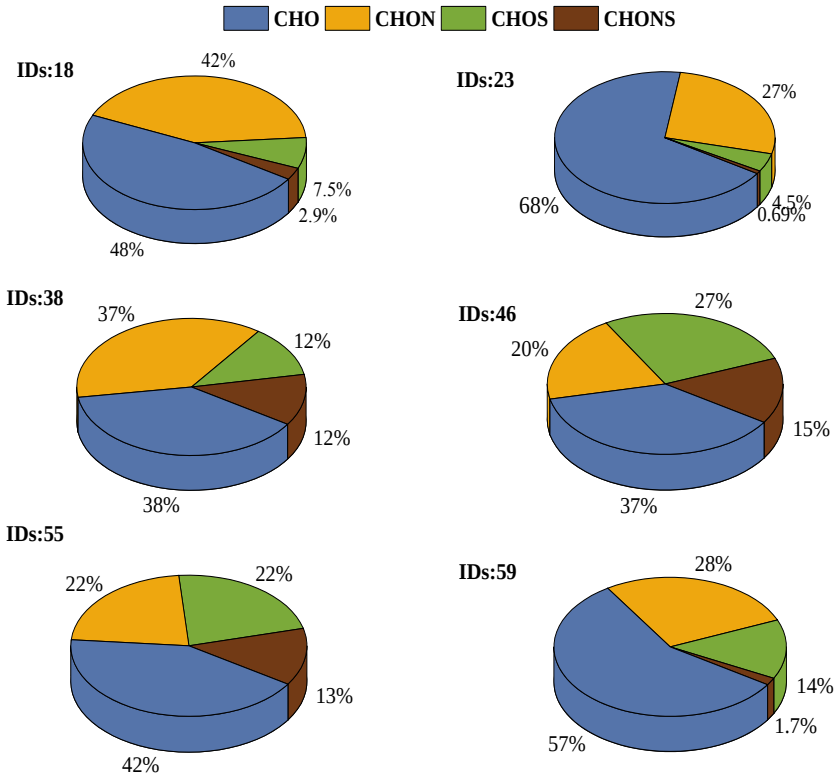

Figure S9. The relative intensity of four types of elemental formulas in WSOC fraction in six samples of three origins: CHO- and CHON-group were the main species in all extract, while S-contained compounds only presented higher fraction in coal combustion and vehicle emission.

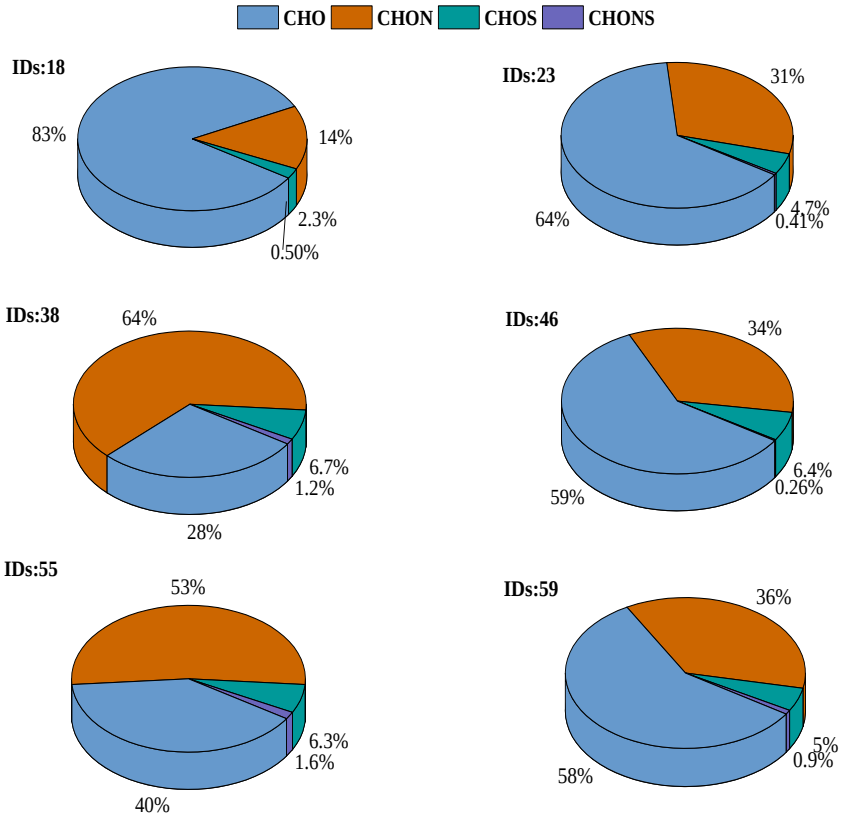

Figure S10. The relative intensity of four types of elemental formulas in MSOC fraction in six samples of three origins: CHO- and CHON-group were the abundance substances in this phases derived from three origins, while S-contained compounds mainly presented in WSOC fraction of coal combustion and vehicle emission, not rich in MSOC fractions

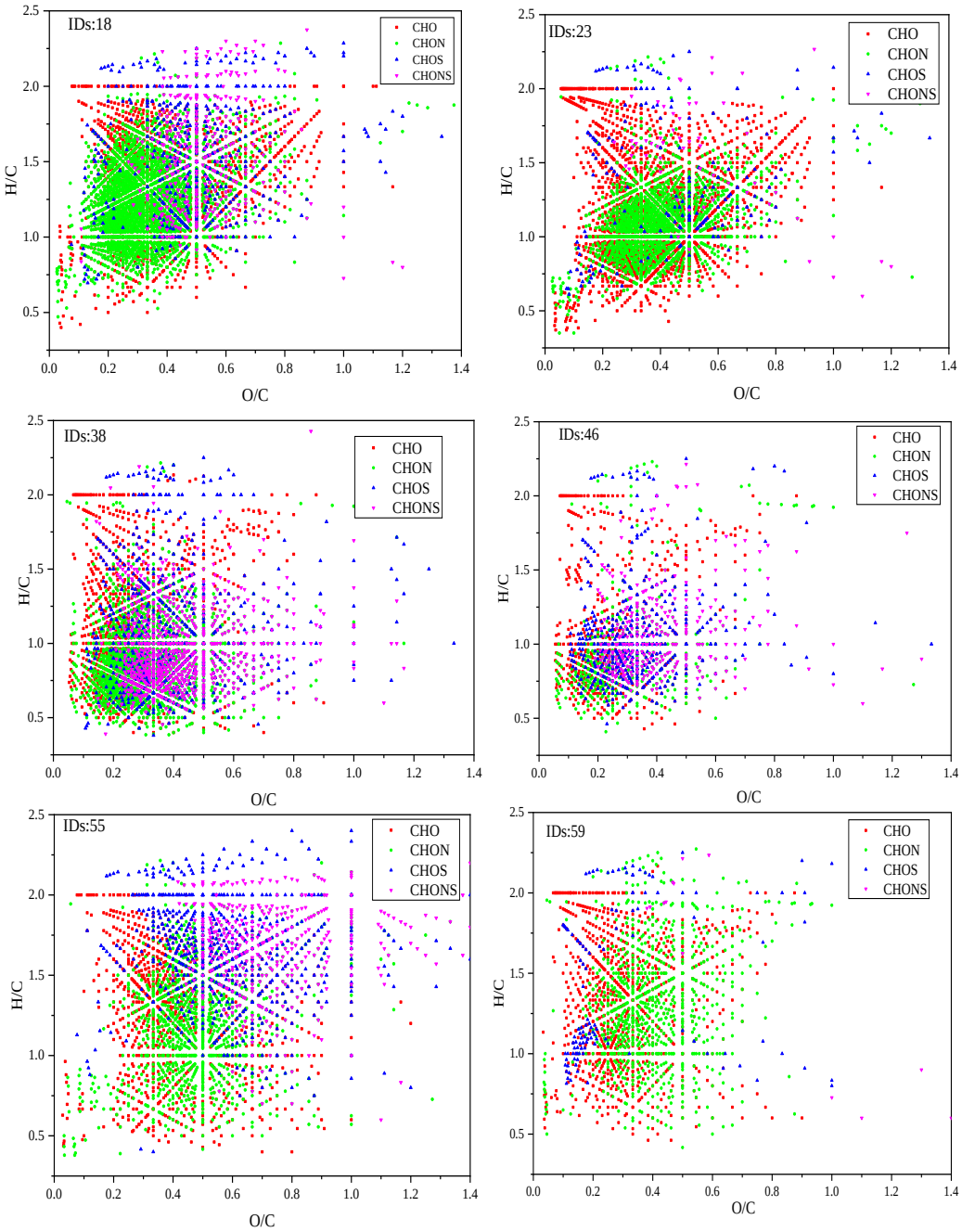

Figure S11. Van Krevelen diagrams of four groups (CHO, CHON, CHOS, and CHONS) in WSOC fraction of three origins; The different regions, identified by the H/C and O/C values, are listed according to the following criteria: lipids (O/C=0-0.2, H/C=1.7-2.2), proteins (O/C=0.2-0.6, H/C=1.5-2.2, N/C≥0.05), lignin (O/C = 0.1−0.6, H/C =0.6−1.7, AI_{mod} < 0.67), carbohydrates (O/C = 0.6−1.2, H/C = 1.5−2.2), tannins (O/C = 0.6−1.2, H/C = 0.5−1.5, AI_{mod} < 0.67), and unsaturated hydrocarbons (O/C = 0−0.1, H/C = 0.7−1.5) (Patriarca et al., 2018)

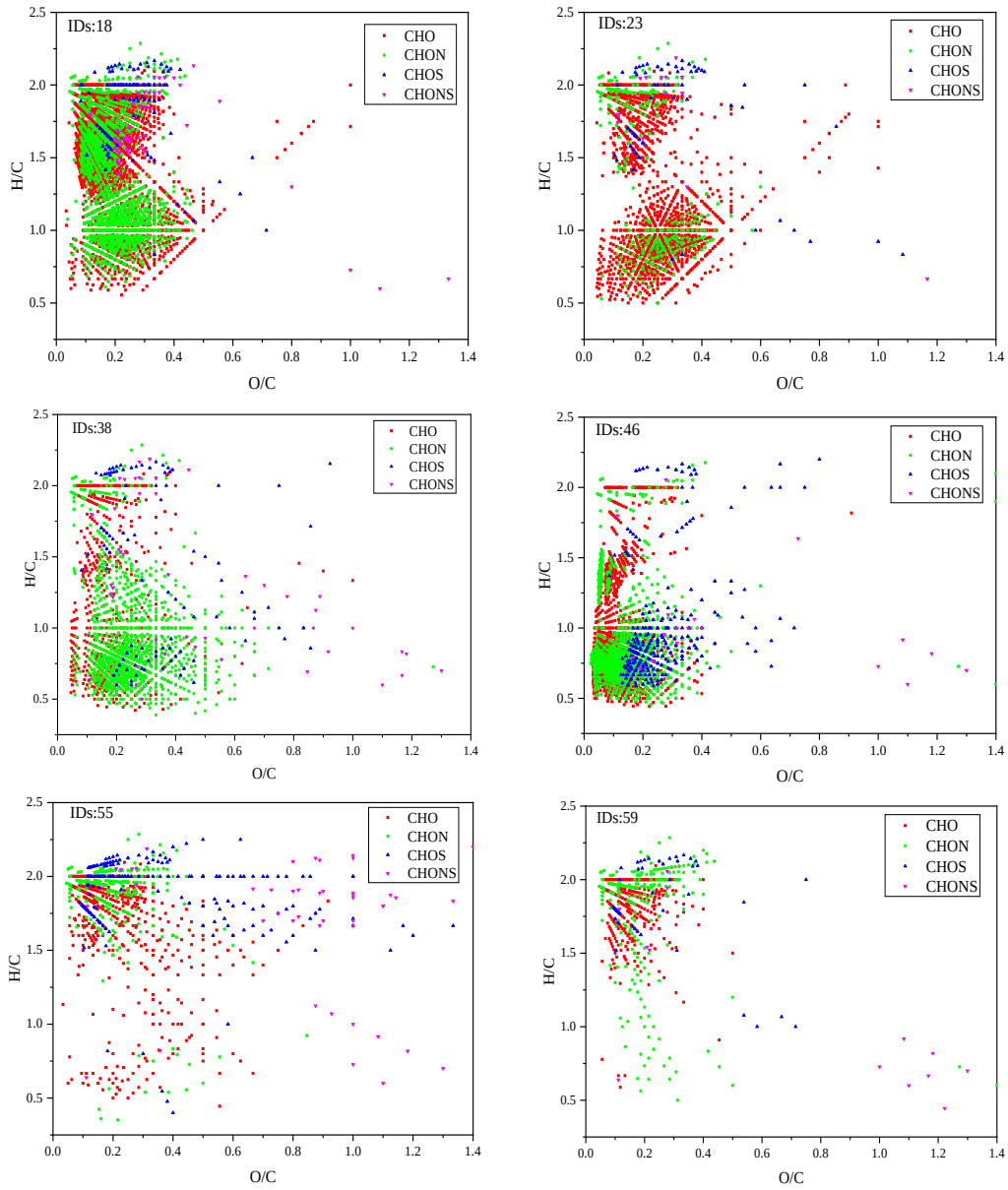

Figure S12. Van Krevelen diagrams of four groups (CHO, CHON, CHOS, and CHONS) in MSOC fraction of three origins

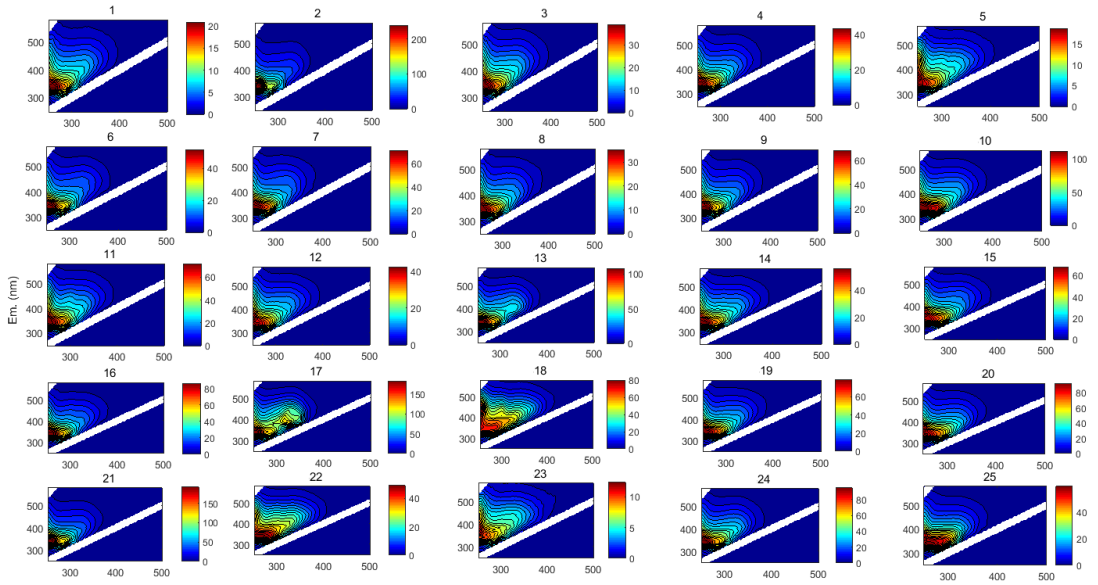
Em. (nm)

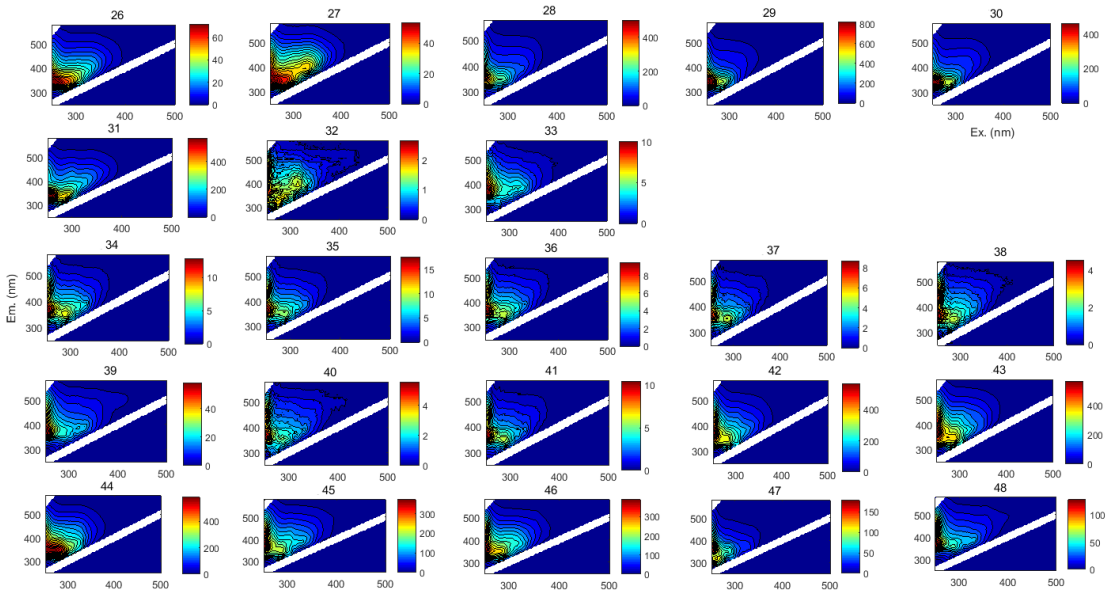
Ex. (nm)
Em. (nm)

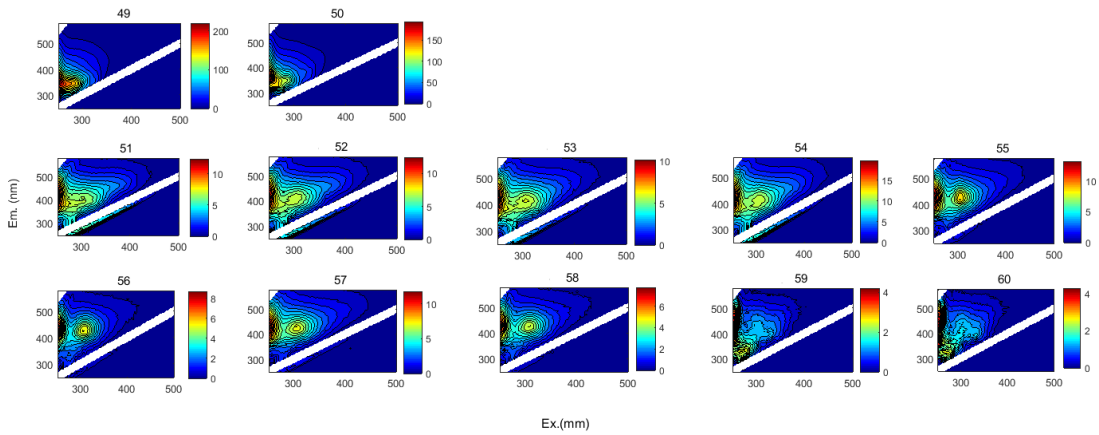
Em. (nm)
Ex.(mm)

Figure S13. The EEM spectra of WSOC fraction of three origins: IDs: 1-33 for biomass burning, IDs: 34-50 for coal combustion, and IDs: 51-60 for vehicle emission.

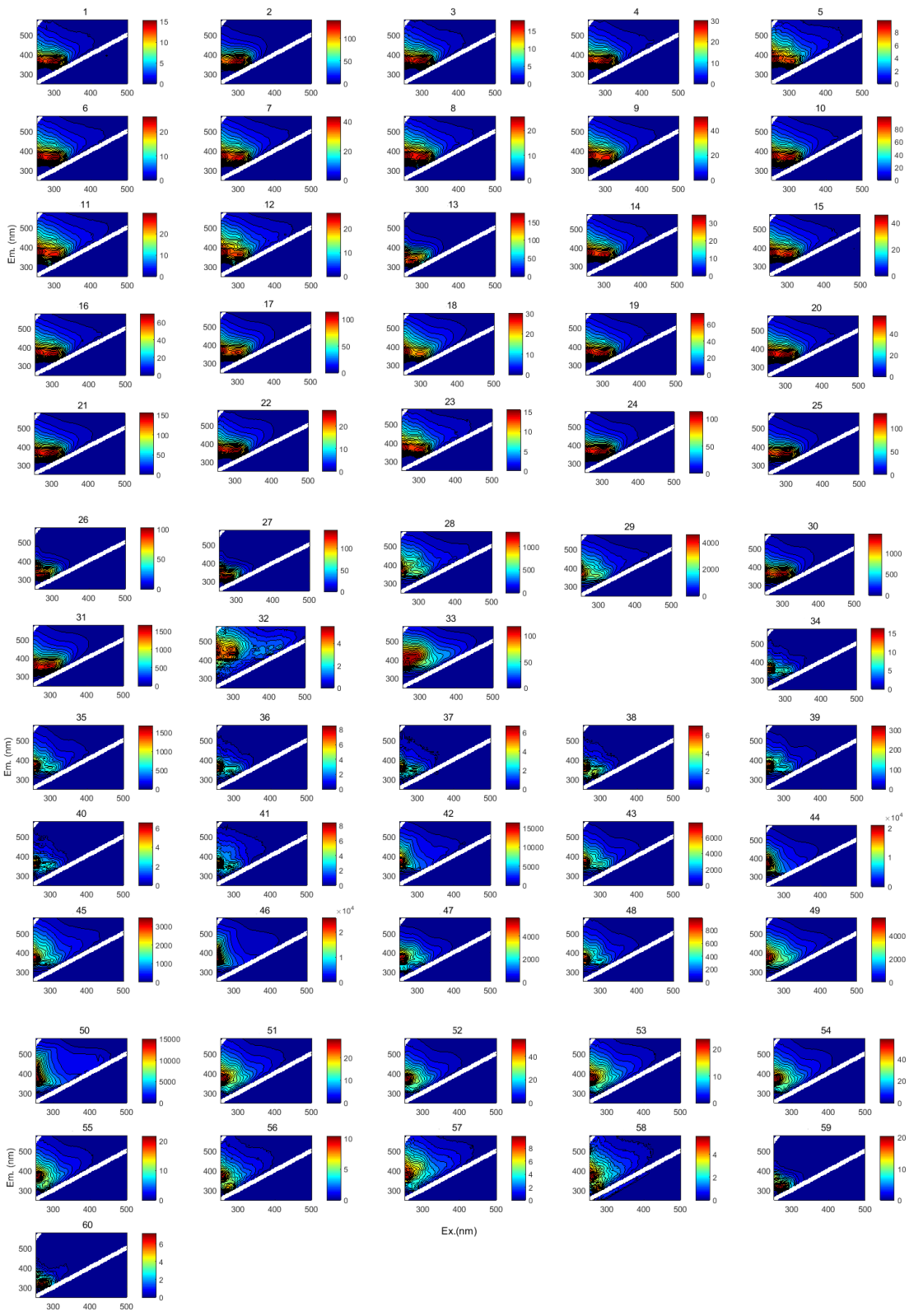

Figure S14. The EEM spectra of MSOC fraction in three origins: IDs: 1-33 for biomass burning, IDs: 34-50 for coal combustion, and IDs: 51-60 for vehicle emission.